ACS OMEGA

http://pubs.acs.org/journal/acsodf

Article

Facile Room-Temperature Synthesis of Cerium Carbonate and Cerium Oxide Nano- and Microparticles Using 1,1′-Carbonyldiimidazole and Imidazole in a Nonaqueous Solvent

Seung Woo Choi and Jaeyun Kim*

Cite This: *ACS Omega* 2021, 6, 26477−26488

Read Online

ACCESS | Metrics & More | Article Recommendations | Supporting Information

ABSTRACT: Ceria nanoparticles (CeONPs) are versatile materials due to their unique catalytic properties, and cerium carbonate particles (CeCbPs) have been widely used as precursors for cerium oxide due to their ease of production. Urea is a widely used precipitant and a source of carbonate ions for the synthesis of CeONPs and CeCbPs, and the reaction temperature is important for controlling the rate of urea decomposition. However, the precise control of the temperature is often difficult, especially in large-scale reactions. Herein, we propose a homogeneous precipitation method that uses 1,1′-carbonyldiimidazole (CDI) and imidazole in acetone without heating. The decomposition rate of CDI can be controlled by the amount of water in the reaction mixture. In the synthesis of CeCbPs, unique particle morphologies of plate-, flying-saucer-, and macaron-like shapes and a wide range of sizes from 180 nm to 13 μm can be achieved by adjusting the amount of CDI, imidazole, and water in the reaction. These CeCbPs are transformed into ceria particles by calcination while maintaining their characteristic morphology. Moreover, the direct synthesis of 130 nm spherical CeONPs was possible by decreasing the amount of CDI in the reaction and the mixing time. These nanoparticles exhibited higher production efficiency and superior reactive oxygen species (ROS) scavenging properties compared to the other CeONPs obtained from calcination. These results demonstrate a novel method using CDI and imidazole in the synthesis of CeONPs and CeCbPs without the aid of a heating process, which may be useful in the large-scale synthesis and application of CeO nanomaterials.

1. INTRODUCTION

Cerium oxide (ceria, CeO_2), one of the most versatile rare-earth materials, has received significant attention, owing to its unique physicochemical and catalytic properties in a variety of applications, including industrial catalysis,[1] polishing agents,[2] photocatalysis,[3] oxygen storage materials,[4] and electrolytes for solid oxide fuel cells.[5] In particular, its catalytic properties can be greatly improved by reducing the size to a nanoscale, which can generate more oxygen vacancies on the surface of nanoparticles, owing to the coexistence of Ce^{3+} and Ce^{4+} oxidation states.[6−8] Due to their highly efficient catalytic properties that mimic those of catalase (CAT) and superoxide dismutase (SOD),[9,10] cerium oxide nanoparticles (CeONPs) have recently expanded their application to the biomedical area, including the theragnostics of systemic inflammatory diseases,[11−13] hepatic diseases,[14,15] brain diseases,[16−18] and eye diseases.[19,20]

Cerium carbonates (CeCbs), including cerium hydroxycarbonate ($CeOHCO_3$), cerium oxycarbonate hydrate ($Ce_2O(CO_3)_2 \cdot H_2O$), and cerium carbonate octahydrate ($Ce_2(CO_3)_3 \cdot 8H_2O$), have been widely investigated as precursors of cerium oxide, owing to their facile synthesis and ease of scalable production.[21−23] In addition, distinctive morphologies of nano- and microparticles composed of cerium oxides, such as shuttle-, butterfly-, flower-, and globin-like particles,[24−26] can be achieved through their synthesis using CeCb as a precursor, making them powerful synthetic alternatives that enhance desirable and controllable physicochemical and catalytic properties.[22,27]

Urea is a widely used chemical component as a precipitating agent and a source of carbonate ions in various synthetic methods for cerium carbonate, such as the urea homogeneous precipitation method,[21,28] hydrothermal synthesis,[29,30] sonochemical synthesis,[31] and microwave-hydrothermal method.[32] Urea can be decomposed into ammonium and carbonate ions by hydrolysis and the rate of urea decomposition is governed by the reaction temperature.[21,33] Compared to other synthetic

Received: July 13, 2021
Accepted: September 9, 2021
Published: September 28, 2021

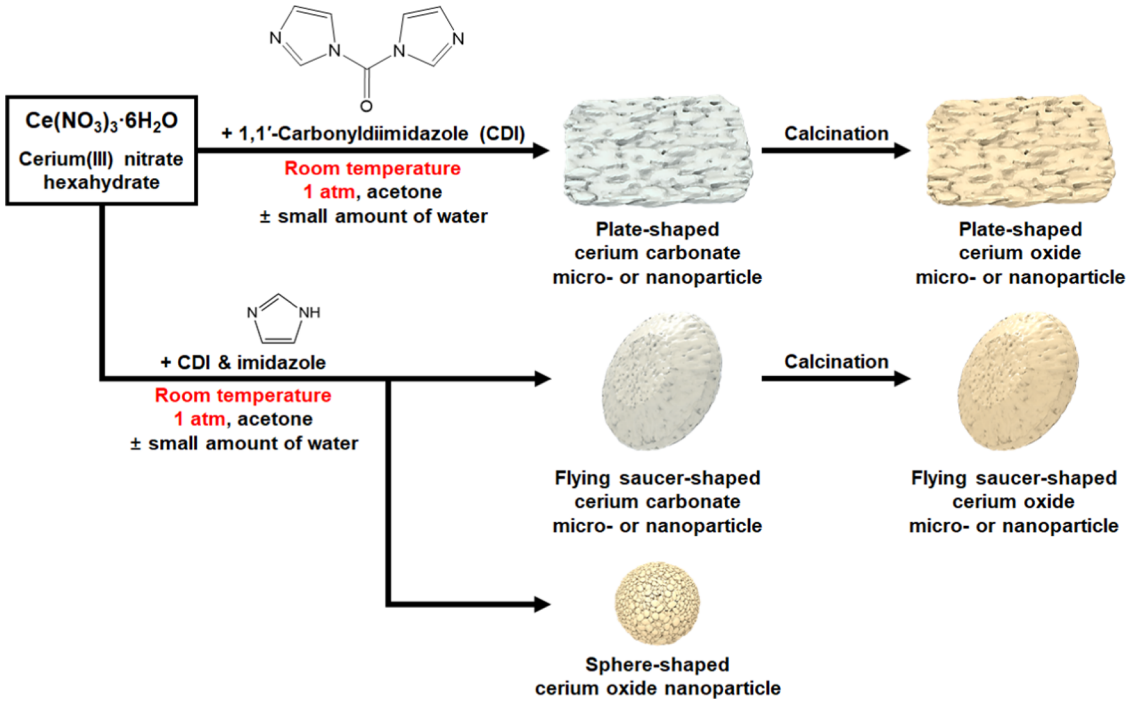

Figure 1. Schematic illustration of the synthetic process for cerium carbonate (CeCb) micro- or nanoparticles and CeONPs by controlling the amounts of CDI and imidazole in acetone at room temperature.

routes, the urea homogeneous precipitation method does not require a special instrument, such as an autoclave, microwave device, or ultrasonic probe, which is beneficial for the facile and inexpensive preparation of CeCb particles. However, it usually requires additional heating and long reaction times to achieve appropriate urea decomposition rates. Urea is also commonly used in various synthetic methods for preparing CeONPs. As in the case of CeCb, urea can act as a precipitating agent in the synthesis of CeONP via thermal decomposition.[34,35] In the hydrothermal synthesis of CeONPs, urea can act as either a reducing agent[36] or a supporting substance for crystal growth.[37] In addition, urea can act as a fuel for exothermic reactions in a microwave-assisted combustion method.[38] Although urea is commonly used for the synthesis of CeCb and CeONPs, a heating process to induce the decomposition of urea is necessary. Therefore, a synthetic method that does not need heat can be an option to shorten the reaction time and increase the preparation efficiency of CeCb and CeONPs.

1,1′-Carbonyldiimidazole (CDI) is a useful coupling agent for the formation of amide bonds and carbamate bonds.[39−41] CDI decomposes into imidazole and carbon dioxide very quickly by hydrolysis at room temperature.[42] Imidazole resulting from the decomposition of CDI is a key component in the synthesis of various imidazole-coordinated metal complexes, including imidazolate-bridged copper(II) complex,[43,44] imidazole-coordinated cadmium(II) complex,[45] imidazole-coordinated cobalt(II) complex,[46] and zeolitic imidazolate frameworks (ZIFs).[47−49] Recently, a coprecipitation method for the synthesis of a CeONP-decorated cerium(III)−imidazole network at room temperature with CDI has been reported.[50] Although this report shows the potential of using cerium compounds and imidazole derivatives to synthesize CeONPs, CeONPs can only be obtained in a mixed form with a cerium−imidazole network. Moreover, most reports focus on the reaction of metal ions with imidazoles derived from CDI decomposition. The role of carbon dioxide, the other chemical component derived from CDI decomposition, as a source of carbonate ions in various chemical reactions has not received scientific attention.

In the present study, we propose a facile and rapid method for synthesizing CeCb nano- and microparticles and CeONPs at room temperature without heating, using CDI and imidazole in acetone (Figure 1). CDI acts as a carbonate source (via carbon dioxide) as well as a precipitating agent (via imidazole) after its decomposition. Due to the fast and controllable decomposition of CDI depending on the amount of water in the acetone solution, CeCb particles of diverse sizes ranging from around 180 nm to 13 μm could be prepared without a heating process within a relatively short mixing time (~3 h). The morphology of CeCbNPs could be varied from a nanoplate to a flying-saucer shape (nanosaucer) by adding imidazole and adjusting the amount of CDI. The CeCbNPs could be converted into CeONPs via calcination while maintaining their morphology. In addition, we have demonstrated the direct synthesis of uniform CeONPs with high ROS-scavenging properties in the presence of CDI and additional imidazole. This method may provide a useful methodological tool for designing nanoparticles and microparticles composed of cerium carbonate and cerium oxide with an efficient synthetic process and numerous applications.

2. RESULTS AND DISCUSSION

To investigate the effect of CDI on the formation of particles, cerium nitrate hexahydrate was reacted with various concentrations of CDI and the speed of precipitation was observed. A relatively small amount of CDI (0.5 and 1 mmol) led to slow precipitation, while higher CDI amounts (2 and 4 mmol) clearly showed rapid precipitation (Video S1, Supporting Information). The actual time scale for the occurrence of precipitation ranged from a few seconds to tens of minutes

https://doi.org/10.1021/acsomega.1c03700
ACS Omega 2021, 6, 26477−26488

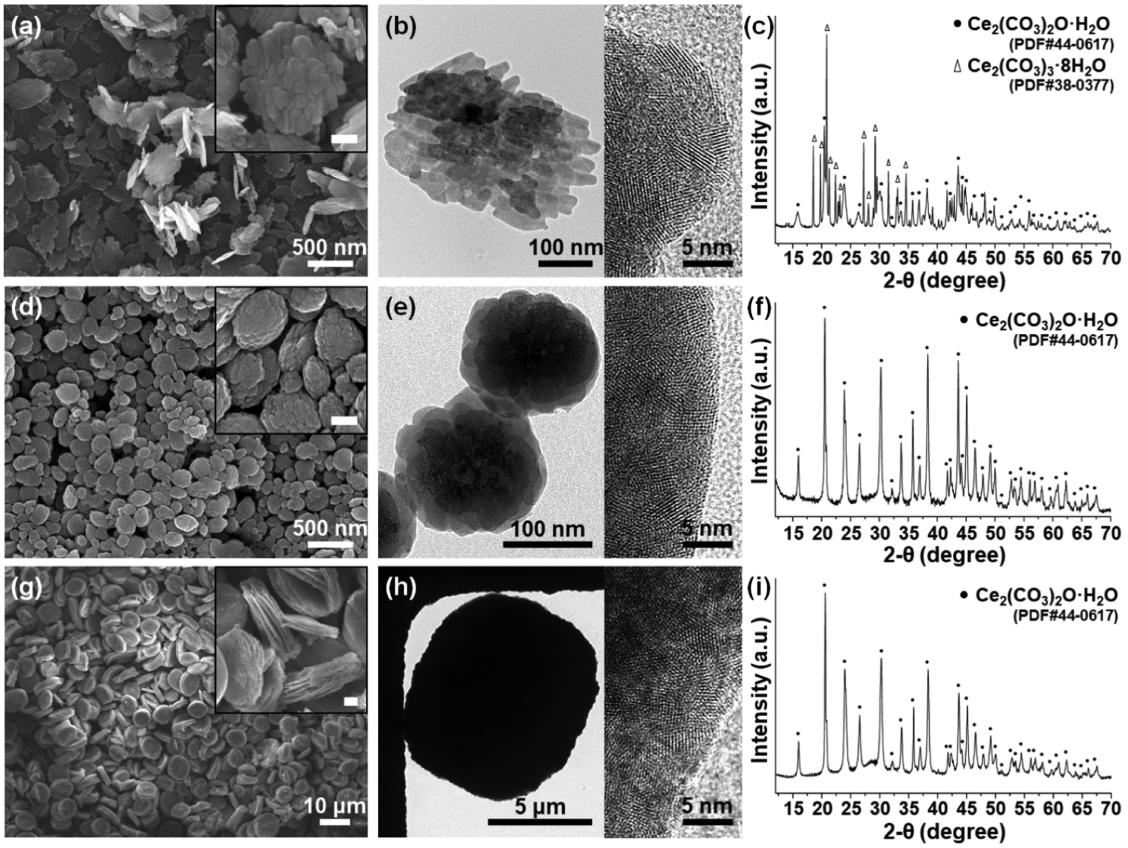

Figure 2. Morphological and structural characteristics of CeCb particles. SEM (a, d, g), TEM (b, e, h), and XRD (c, f, i) results of (a−c) CeCb nanoplates, (d−f) CeCb nanosaucers, and (g−i) macaron-shaped CeCb microparticles obtained from addition of 1000 μL of deionized water. Scale bars of the inset: 100 nm for (a) and (d) and 1 μm for (g).

(Figure S1, Supporting Information). Scanning electron microscopy (SEM) images revealed that microsized aggregation occurred with small amounts of CDI (Figure S2, Supporting Information), but the shape of the particles changed dramatically into nanoplates 350 nm in diameter and 35 nm in thickness as the amount of CDI increased (Figure 2a). The magnified SEM images show that the nanoplates are composed of an assembly of smaller rod-shaped 67 × 33 nm nanoparticles, and it is confirmed from the transmission electron microscopy (TEM) images that these smaller rod-shaped nanoparticles are made up of about 4-nm-sized nanoparticles (Figure 2b). X-ray diffraction (XRD) analysis shows that the nanoplates are composed of mixed phases of cerium oxycarbonate ($Ce_2(CO_3)_2O·H_2O$, PDF #44-0617) and cerium carbonate hydrate ($Ce_2(CO_3)_3·8H_2O$, PDF #38-0377) (Figure 2c). As the amount of CDI increases, the peak intensity of cerium carbonate hydrate increases compared to that of cerium oxycarbonate, indicating that the formation of cerium carbonate hydrate is dominant over cerium oxycarbonate in conditions with higher CDI concentrations (Figure S3, Supporting Information). In particular, the peak corresponding to the (020) facet at 10.5° was highly intensified as the amount of CDI increased. To determine whether the amount of generated CO_2 (the carbonate source) correlates with the amount of CDI, the amounts of dissolved CO_2 in acetone were measured by a titration kit (Figure S4, Supporting Information). Although this kit was optimized for measuring dissolved CO_2 in aqueous solutions, it was able to measure the relative amount of CO_2 contained in acetone indirectly. As the amount of CDI increased, the amount of dissolved CO_2 in acetone increased, which means that CO_2 dissolved in acetone, which can serve as a carbonate source, is derived from the decomposed CDI.

Since it is known that imidazole is a byproduct from the hydrolysis of CDI and participates in the precipitation, we hypothesize that the presence of imidazole prior to CDI decomposition may affect the formation of CeCb particles. To investigate the effect of imidazole, additional imidazole (6 mmol) was added to the reaction mixture of cerium nitrate hexahydrate and CDI in acetone and the precipitation was characterized. As extra imidazole was added, the morphology and particle size changed significantly. The resulting nanoparticles show a morphology of flying saucers (nanosaucers) composed of assembled smaller particles and the size of the nanosaucers is 176 ± 42 nm (Figures 2d,e and S5, Supporting Information). When larger amounts of extra imidazole (4 and 6 mmol) are added, the size of the nanosaucers decreases without any significant morphological differences compared to the reaction to which a smaller amount of extra imidazole (2 mmol) was added. However, there was no significant difference in size between the reaction products to which 4 or 6 mmol of imidazole was added, indicating that adding more than a certain amount of imidazole no longer affects the size reduction of the particles (Figure S6, Supporting Information). XRD patterns exhibiting representative peaks corresponding to the (110), (111), (102), (131), and (221) facets at 20.6, 23.9, 30.3, 38.4, and 43.7°, respectively, show that the nanosaucers can be assigned to $Ce_2(CO_3)_2O·H_2O$ (PDF #44-0617) (Figure

https://doi.org/10.1021/acsomega.1c03700
ACS Omega 2021, 6, 26477−26488

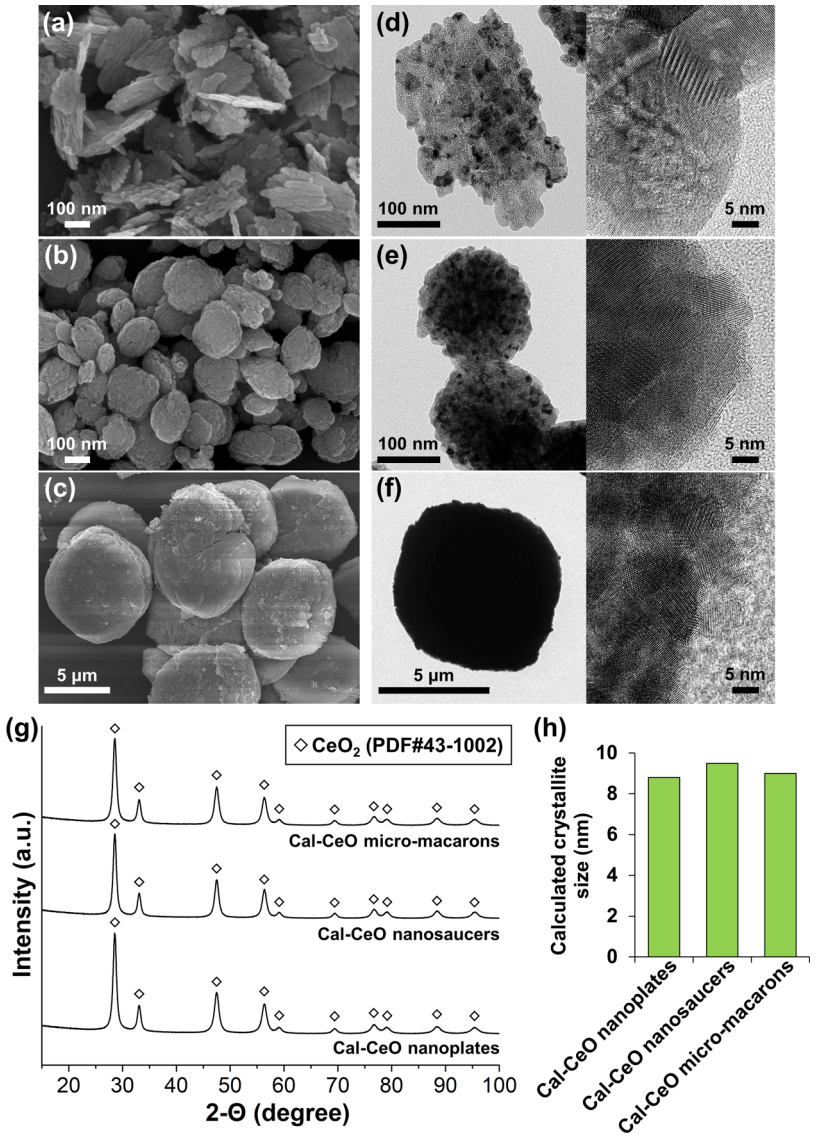

Figure 3. Morphological and structural characteristics of Cal-CeO particles. SEM (a–c) and TEM (d–f) images of (a, d) Cal-CeO nanoplates, (b, e) Cal-CeO nanosaucers, and (c, f) Cal-CeO micromacarons obtained from the addition of 1000 μL of deionized water. (g) XRD patterns and (h) calculated crystallite sizes of Cal-CeO particles.

2f), revealing that these nanosaucers consist of cerium oxycarbonate regardless of the amount of imidazole added (Figure S7, Supporting Information). Imidazole can be formed through the slow hydrolysis of CDI and act as a weak base in the case of the reaction of cerium nitrate hexahydrate and CDI,[51,52] which can induce the slow formation of $Ce_2(CO_3)_3$ from a weak basic condition.[53] However, the addition of extra imidazole may increase the pH of the reaction mixture more quickly, and formation of $Ce_2(CO_3)_2O{\cdot}H_2O$ can be more favored through the reaction of $2Ce^{3+} + 2OH^- + 2CO_3^{2-} \rightarrow Ce_2(CO_3)_2O{\cdot}H_2O$.[54,55] Taken together, these results show that the addition of extra imidazole not only transforms the morphology of CeCb nanoparticles from nanoplates (Figure 2a,b) to nanosaucers (Figure 2d,e) but also changes their phase composition from cerium carbonate hydrate ($Ce_2(CO_3)_3{\cdot}8H_2O$) (Figure 2c) to cerium oxycarbonate ($Ce_2(CO_3)_2O{\cdot}H_2O$) (Figure 2f).

In the urea homogeneous precipitation method, it is known that reaction temperature can control the decomposition rate of urea into NH_4^+, OH^-, and CO_3^{2-} ions by hydrolysis and subsequently control the precipitation process owing to an increase in alkalinity.[21] Therefore, it has been reported that the shape and size of nanoparticles can be changed by controlling the reaction temperature in the urea homogeneous precipitation method.[56,57] In a similar vein to the case of urea, we wanted to know whether controlling the decomposition rate of CDI affects the structure of the nanoparticles in the present study. Based on this, we further investigated whether controlling the decomposition rate of CDI can affect the formation of CeCb particles. To control the decomposition rate of CDI without using heat, we used the extra addition of small amounts of water in the reaction mixture, as CDI can decompose rapidly into imidazole and carbon dioxide in the presence of water.[41] Although acetone was used as a solvent in the present study, the reaction mixture contained a small amount of water derived from cerium nitrate hexahydrate and 99.5% acetone and this water is capable of decomposing the CDI. This led us to investigate the effect of the addition of extra water on nanoparticle formation.

https://doi.org/10.1021/acsomega.1c03700
ACS Omega 2021, 6, 26477−26488

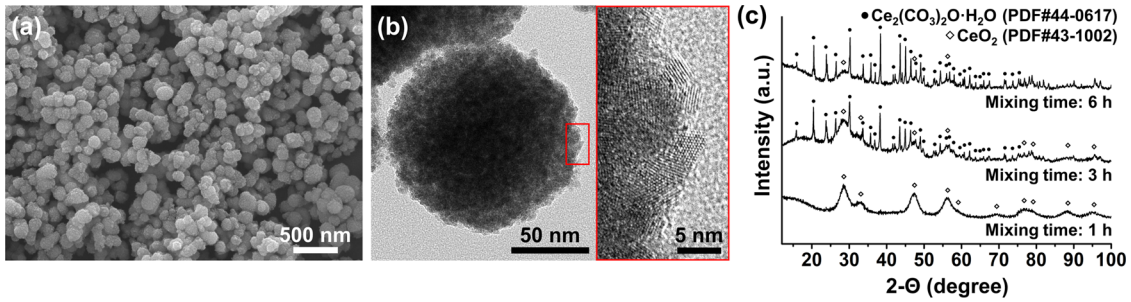

Figure 4. (a) SEM and (b) TEM images of Ce-CDI-IM CeONPs (mixing time: 1 h; red box: magnified image). (c) XRD patterns of the reaction products (Ce/CDI/imidazole = 1:0.5:4 mmol in the reaction) according to the mixing time from 1 h (Ce-CDI-IM CeONPs) to 6 h.

When more water was added in the reaction mixture of cerium nitrate hexahydrate and CDI, the precipitation occurred more rapidly (Video S2, Supporting Information). SEM images of the precipitate obtained with addition of different amounts of water (0.3, 0.6, 1.0, 1.3 mL) in the reaction mixture of CeCb nanosaucers in the presence of 6 mmol imidazole showed that the particle size increases dramatically to a range of 412 nm to 13.6 μm (Figures 2g,h, S8, and S9, Supporting Information). When a relatively small amount of water was added, the overall morphology of particles remained similar to the CeCb nanosaucers prepared without the use of additional deionized water. When a larger volume of deionized water was added, characteristic macaron-like microparticles were observed with a layered structure that was somewhat squashed. The macaron-like microparticles prepared with 1000 μL of deionized water showed the XRD pattern of cerium oxycarbonate $Ce_2(CO_3)_2O{\cdot}H_2O$, indicating that there was no phase change regardless of the addition of deionized water during the reaction (Figure 2i). In the absence of extra imidazole to prepare the CeCb nanoplates, the addition of extra water showed a similar tendency of increasing the particle size according to the amount of deionized water added, but the overall plate shape was maintained without a significant change (Figure S10, Supporting Information). To verify the effect of water added into the reaction mixture, the change in the amount of CO_2 generated according to the change in the amount of water was indirectly evaluated by counting the CO_2 bubbles generated during the reaction[58] and titrating the amount of NaOH consumed due to the CO_2 dissolution after the reaction (Figure S11, Supporting Information).[59] As the amount of water added to the cerium salt-free acetone solution increased, the amount of CO_2 generated during the reaction increased. In addition, the generated CO_2 from the reaction can react with NaOH in a different reactor to form $NaHCO_3$ and the amount of NaOH consumed can be measured by titration with HCl.[59] In the case of adding a large amount of water, the amount of NaOH consumed was plenty compared to the reaction to which a smaller amount of water was added, indicating that the addition of water could be the important factor accelerating the decomposition of CDI. The addition of cerium nitrate hexahydrate to the reaction mixture decreased the amount of CO_2 generated, suggesting that some of the CO_2 generated was consumed to form reaction products in the reaction. Taken together, these results indirectly showed that the addition of water can accelerate the production of CO_2 by faster decomposition of CDI and that this generated CO_2 can participate in the reaction as a reactant.

The result of adding water in the CeCb particle formation process is contrary to previous reports that describe faster nucleation by rapid decomposition of urea at high reaction temperature that leads to the formation of smaller size particles in the urea homogeneous precipitation method.[60,61] However, the particle size synthesized at 70 °C by the urea homogeneous precipitation method could be smaller due to incomplete urea decomposition.[21,60] Similarly, incomplete and slow decomposition of CDI in the reaction mixture containing small amounts of water may be one of the reasons for the smaller-sized CeCb particles. On the other hand, it has been reported that the particle size increases with longer reaction times due to continuous growth of the particles and a more complete reaction.[61,62] In our study, since burst precipitation already occurred owing to the presence of extra imidazole early in the synthesis of the CeCb nanosaucers, deionized water added to the reaction mixture may serve to increase the reaction time by rapidly producing reactants at the beginning of the reaction due to the induction of rapid decomposition of the CDI. However, further studies are needed to confirm the possibility that water participates not only in the decomposition of CDI but also in the reaction with other reactants directly.

Cerium carbonate is known as a good precursor for conversion into cerium oxide. CeCb nanoplates, CeCb nanosaucers, and macaron-shaped CeCb microparticles were calcined in air (Cal-CeO particles) and the resulting powders were characterized by SEM, TEM, and XRD. Despite the CeO_2 conversion process at high temperature (500 °C), the original morphologies of nanoplates, nanosaucers, and macaron-shaped microparticles were well maintained with the assembly of smaller subunits (Figure 3a−c).[23] The TEM images also showed that the Cal-CeO particles were composed of subunits of nanoparticles, similar to the case of CeCb particles, but the size of nanoparticles increased due to calcination (Figure 3d−f). XRD analysis of all calcined particles showed that the typical CeO_2 phase of a cubic fluorite structure with high crystallinity was obtained after calcination (Figure 3g).[63] The calculated crystallite sizes by the Debye−Scherrer equation using XRD data showed comparable values between Cal-CeO particles (Figure 3h). Then, we further investigated the effect of the calcination temperature and the heating rate on the properties of Cal-CeONPs (Figure S12, Supporting Information). There was no definite morphological change according to the changes in the calcination temperature and the heating rate. However, as the calcination temperatures increased, the XRD peaks with a cubic fluorite structure of cerium oxide became sharper, and the crystallite sizes increased from 4.9 nm at 300 °C to 9.3 nm at 500 °C. In addition, the effect of the heating rate seemed to

https://doi.org/10.1021/acsomega.1c03700
ACS Omega 2021, 6, 26477−26488

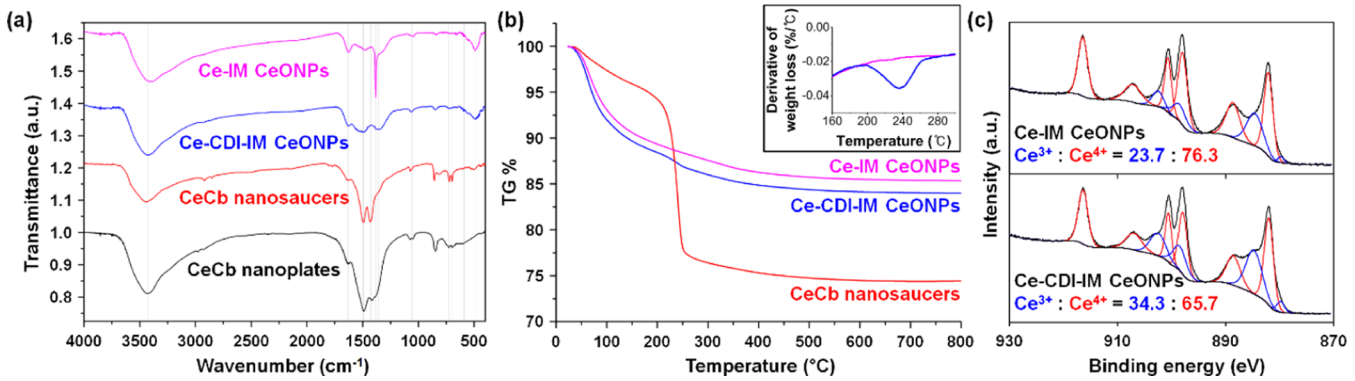

Figure 5. Structural characteristics of various types of nanoparticles for comparison of Ce-IM CeONPs and Ce-CDI-IM CeONPs. (a) FTIR spectra, (b) TGA results (inset: derivative thermogravimetry (DTG) of Ce-IM and Ce-CDI-IM CeONPs), and (c) Ce 3d X-ray photoelectron spectroscopy (XPS) analysis.

be small compared to the calcination temperature, as previously reported for other nanoparticles.[64] The plate shape of cerium oxide has recently attracted attention owing to its UV-shielding effect and pearlescence in cosmetic applications, but the synthesis of plate-shaped particles composed of cerium oxide is not as easy, owing to its crystal structure.[65] In this regard, the synthesis of ceria nanoplates using CeCb nanoplates as precursors can be further investigated for potential applications in cosmetics.

In biological applications, nanoparticles of about 100 nm in size are known to have the advantage of exhibiting prolonged circulation time and efficient drug delivery to target sites such as tumors.[66] We further controlled and optimized the reaction parameters (CDI, imidazole, water, mixing time) in the synthesis of CeCb nanosaucers to investigate if we could achieve the fabrication of smaller and more uniform nanoparticles suitable for biomedical applications. In the case of further reducing the amount of CDI from 1 to 0.5 mmol in the reaction mixture of acetone and imidazole without adding deionized water, a mixture of plate-shaped microparticles and spherical nanoparticles (130−200 nm size according to the amount of imidazole) were obtained after a mixing time of 3 h (Figure S13, Supporting Information). When the mixing time was decreased to 1 h (Ce-CDI-IM CeONPs), uniform spherical nanoparticles that averaged 130 nm in size were obtained without microparticles, different from the reaction products with longer mixing times (Figures 4a and S14, Supporting Information). TEM analysis revealed that these 130 nm nanoparticles are composed of an assembly of small nanoparticles with a size of a few nm (Figure 4b). In the SEM image of the product separated 1 min after the start of the reaction of the synthesis of Ce-CDI-IM CeONPs, small subunits of nanoparticles with a size of about 13 nm were observed (Figure S15, Supporting Information). As the size of nanoparticles decreases, the surface energy increases due to an increase in dangling bonds and defects on the surface of the nanoparticles.[67,68] Therefore, the reaction may have progressed in the direction of forming 130-nm-sized nanoparticles, which can be called aggregates.[68] XRD analysis of the 130 nm nanoparticles obtained from short mixing time (1 h) exhibits representative peaks at 28.4, 33.0, 47.5, and 56.3°, corresponding to the (111), (200), (220), and (311) facets of CeO_2 (PDF #43-1002), respectively, and the average crystalline size using the Debye−Scherrer equation is 3.1 nm (Figure 4c). Taken together with the TEM observations, it is clear that the 130 nm CeONPs are an assembled form of 3-nm-sized small nanoparticles. As the mixing time increases, the XRD peaks assigned to the phase of $Ce_2(CO_3)_2O{\cdot}H_2O$ appear to be mixed with peaks for CeO_2. Based on SEM and XRD data, the identity of the microparticles in the reaction products at higher mixing times is cerium oxycarbonate. Taken together, these results showed that CeONPs can be directly synthesized from the reaction of cerium nitrate hexahydrate, CDI, and imidazole in acetone at room temperature at short mixing times.

To understand the role of CDI in the Ce-CDI-IM CeONPs, we prepared nanoparticles without addition of CDI in the synthesis of Ce-CDI-IM CeONPs. Interestingly, the resulting precipitate (Ce-IM CeONPs) shows a uniform morphology of 130 nm spherical nanoparticles (Figure S16a, Supporting Information), which are similar to those of Ce-CDI-IM CeONPs. The hydrodynamic size is 296.4 ± 5.0 nm, comparable to that of Ce-CDI-IM CeONPs (297.1 ± 4.6 nm). XRD analysis reveals that the phase of nanoparticles is CeO_2 (PDF #43-1002) and the average size of nanoparticles derived from the Debye−Scherrer equation is 3.0 nm (Figure S16b, Supporting Information). Although similar 130 nm CeONPs were obtained without using CDI, the yield of synthesized Ce-IM CeONPs was much lower than that of Ce-CDI-IM CeONPs. The yield of Ce-CDI-IM CeONPs synthesized from the same amount of cerium salts was 10.6 times higher than that of Ce-IM CeONPs. Although the size and phase of the resulting nanoparticles were similar, the addition of a small amount of CDI in the reaction led to a significantly higher yield.

We further characterized the differences between Ce-CDI-IM CeONPs and Ce-IM CeONPs. In the Fourier transform infrared (FTIR) spectra, peaks corresponding to stretching and bending vibrations of hydroxyl groups on the surface of nanoparticles are observed at 3400 and 1630 cm^{-1}, respectively, for all nanoparticles (Figure 5a).[69] In addition, peaks at 500−600 cm^{-1} for the O−Ce−O stretching vibration,[70,71] peaks at ∼1380 cm^{-1} for the vibration mode of Ce−O−Ce,[72,73] and small peaks at 1050 cm^{-1} for physical absorption of water[74] are also found in all nanoparticles. Peaks for a carbonate ion at 1494 cm^{-1} (ν_{as} O−C−O), 1430 cm^{-1} (ν_{as} O−C−O), 840 cm^{-1} (π−CO_3^{2-}), and 720 cm^{-1} (δ−CO_3^{2-}) are found in the spectra of CeCb nanoplates, CeCb nanosaucers, and Ce-CDI-IM CeONPs, but not in Ce-IM CeONPs.[75,76] In the spectrum of Ce-IM CeONPs, a sharp peak for the presence of nitrate ions on the surface of

https://doi.org/10.1021/acsomega.1c03700
ACS Omega 2021, 6, 26477−26488

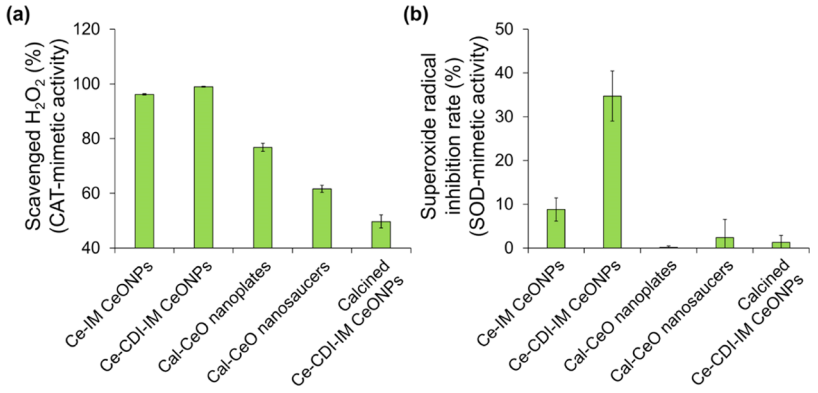

Figure 6. Catalytic characteristics of directly synthesized CeONPs (Ce-IM and Ce-CDI-IM CeONPs) and calcined CeONPs. (a) Catalase (CAT)-mimicking activity confirmed by a hydrogen peroxide/peroxidase assay reacting with 20 μM H_2O_2 for 1 h and (b) SOD-mimicking activity confirmed by a SOD determination assay (amount of each NP in both assays: 100 μg/mL).

nanoparticles appears at 1382 cm^{-1}, suggesting that there is a difference in surface properties between Ce-IM CeONPs and Ce-CDI-IM CeONPs.[70] Thermogravimetric analysis (TGA) analysis shows a similar initial weight loss due to the desorption of water below 200 °C for all particles, and differing weight losses above 200 °C depending on the type of nanoparticles (Figure 5b). For CeCb nanosaucers, a sharp weight loss occurs at 200−300 °C due to the release of carbon dioxide, as previously reported for cerium carbonate.[77] In contrast, smaller weight losses are observed at the same temperature for both CeONPs. Although there is no significant difference in TGA profiles between Ce-CDI-IM CeONPs and Ce-IM CeONPs, a clear weight loss at 200−300 °C is observed for Ce-CDI-IM CeONPs while there is no such weight loss for Ce-IM CeONPs. This is confirmed by the derivative thermogravimetric (DTG) trend (inset of Figure 5b). This means that a small amount of CDI decomposition products are incorporated into Ce-CDI-IM CeONPs.

The catalytic characteristics of CeONPs are attributed to the coexistence of Ce^{3+} and Ce^{4+} oxidation states. In general, the relative percentage of Ce^{3+} oxidation state increases when the size of the nanoparticles decreases, owing to the formation of oxygen deficiencies on the surface of the nanoparticles. As Ce^{3+} and Ce^{4+} ions are ascribed to the superoxide dismutase (SOD) and catalase (CAT) mimetic activity of CeONPs, respectively,[10,78] the ratio of Ce^{3+}/Ce^{4+} oxidation states in Ce-CDI-IM and Ce-IM CeONPs was analyzed through XPS. In the Ce 3d XPS spectrum, Ce-IM CeONPs and Ce-CDI-IM CeONPs show the coexistence of Ce^{3+} and Ce^{4+} oxidation states and these peaks are in good agreement with previous reports (Figure 5c).[79−81] The Ce^{3+} content of Ce-CDI-IM CeONPs is 34.3%, which is higher than 23.7% for Ce-IM CeONPs. In the O 1s spectrum, both CeONPs showed three peaks at 529.5, 531.2, and 532.8 eV, which are attributed to the lattice oxygens of CeO_2, oxygens near the oxygen vacancies, and hydroxyl groups on the surface, respectively.[82−85] However, the relative amount of oxygens in the vicinity of oxygen vacancies of Ce-CDI-IM CeONPs was 41.3%, which was higher than that of Ce-IM CeONPs with 29.6% (Figure S17, Supporting Information). In the N 1s spectrum, there are no peaks at 400 eV corresponding to imidazole for either of the nanoparticles, while a peak at 406.7 eV corresponding to nitrate species is only observed on the surface of Ce-IM CeONPs (Figure S18, Supporting Information).[86−88] This means that the imidazole acts as a precipitating agent but is not a capping agent or an imidazolate linker. These XPS analyses show that the addition of CDI can affect the properties of the nanoparticle surface, especially an increase in the amount of the Ce^{3+} oxidation state, which is known to be an important factor for ROS-scavenging properties.[89]

Finally, we investigated the ROS-scavenging properties of the CeONPs. CAT-mimicking activity related to the amount of Ce^{4+} oxidation state[9] was measured by a hydrogen peroxide scavenging assay and SOD-mimetic activity related to the amount of the Ce^{3+} oxidation state was measured by a superoxide radical inhibition assay (Figure 6a,b). Ce-IM CeONPs and Ce-CDI-IM CeONPs show higher ROS-scavenging properties, compared to calcinated nanoparticles, in the results of both assays. In general, crystallite size increases with an increase in calcination temperature, and ceria nanoparticles with a smaller crystallite size exhibit superior catalytic properties due to an increase in oxygen vacancies as an active catalytic site on the surface of the nanoparticles.[84,90−92] The XRD result of calcined Ce-CDI-IM CeONPs exhibits a highly crystalline cubic fluorite structure of cerium oxide with an average 8.5 nm crystalline size calculated from the Debye−Scherrer equation, indicating that this relatively large crystal size may be responsible for the low catalytic activity (Figure S19, Supporting Information). Therefore, it may be advantageous in terms of improving the ROS-scavenging activities of CeONPs to prepare CeONPs without the calcination process. Moreover, the Ce-CDI-IM CeONPs exhibit more powerful CAT- and SOD-mimetic properties compared to other CeONPs. The high amount of the Ce^{3+} oxidation state in Ce-CDI-IM CeONPs confirmed through XPS analysis could be the main reason for its superior SOD scavenging properties, which may be advantageous for biomedical applications.[93] Taken together, these results indicate that the production of CeONP, which exhibits higher production efficiency and superior ROS-scavenging properties compared to the product obtained in the reaction without CDI, can be achieved using a small amount of CDI in the reaction of cerium compounds and imidazole.

In the urea homogeneous precipitation method, which is widely used as a synthetic route for inorganic nanoparticles including cerium-containing materials,[94,95] a heating process is essential to achieve proper decomposition of the urea during the reaction. However, it is often difficult to control the temperature precisely for a long time and this could be an obstacle for the control of industrial-scale production of

https://doi.org/10.1021/acsomega.1c03700
ACS Omega 2021, 6, 26477−26488

Table 1. Information about Conditions for the Synthesis of Each Particle

	cerium nitrate hexahydrate	CDI (mmol)	imidazole (mmol)	water (μL)	calcination	reaction temperature (°C)	reaction time (h)	composition	experimental labels
CeCb nanoplates	1	4				room temperature	3	cerium carbonate	Figures 2a−c and 5
CeCb nanosaucers	1	1	2, 4 or 6			room temperature	3	cerium carbonate	Figures 2d−f and 5
CeCb plates (+water)	1	4		300 or 1000		room temperature	3	cerium carbonate	
CeCb flying saucers (+water)	1	1	6	300, 600		room temperature	3	cerium carbonate	
Macaron-shaped CeCb microparticles	1	1	6	1000, 1300		room temperature	3	cerium carbonate	Figure 2g−i
Cal-CeO nanoplates	1	4			+	room temperature	3	cerium oxide	Figures 3a,d,g,h and 6
Cal-CeO nanosaucers	1	1	4 or 6		+	room temperature	3	cerium oxide	Figures 3b,e,g,h and 6
Cal-CeO micromacarons	1	1	6	1000	+	room temperature	3	cerium oxide	Figure 3c,f,g,h
Ce-CDI-IM CeONPs	1	0.5	4			room temperature	1	cerium oxide	Figures 4−6
Ce-IM CeONPs	1		4			room temperature	3	cerium oxide	Figures 5 and 6

nanoparticles due to a thermal gradient inside the reactor that can lead to adverse consequences such as reduced particle uniformity.[96] Moreover, the concept of sustainability has recently emerged as an important factor in considering the design of a synthesis process for nanoparticles.[97] Therefore, developing a synthetic process that does not require heating is not only a good alternative for reducing energy consumption but can also increase its applicability to the industry. Synthesis processes conducted at room temperature are known as a way to reduce energy consumption,[98] and, from this point of view, the synthetic method developed here, which reacts CDI and imidazole in acetone at room temperature for the synthesis of CeCbPs and CeONPs, could be an attractive route for the homogeneous precipitation method. However, although the mixing process is thought to be faster than the heating process, which can be relatively slow because it is transferred through the reactor walls and the part of the solution,[99] inadequate or slow mixing can cause problems that degrade the quality of the nanoparticles and lead to poor batch-to-batch reproducibility.[100,101] Therefore, further studies will be needed to clarify the influence of parameters related to the mixing process in the synthetic method presented here.

3. CONCLUSIONS

Nanoparticles composed of CeCb with distinctive morphologies were successfully synthesized by a facile method, which used CDI and imidazole with cerium nitrate hexahydrate in an acetone environment without any heating process. The particle morphology could be transformed in various ways and the size could be controlled from a nanoscale to microscale by adjusting the amount of CDI, imidazole, and deionized water, or by controlling the mixing time. These CeCbPs were transformed into particles composed of cerium oxide while maintaining their characteristic morphologies in air at 500 °C for 2 h. Moreover, CeONPs could be obtained simply by reducing the amount of CDI, and incorporating a small amount of CDI into CeONPs could increase their ROS-scavenging properties and improve production efficiency. These findings suggest that the proposed method of using CDI and imidazole in an acetone solvent may be a new alternative method for the synthesis of versatile particles composed of CeCb or cerium oxide, and it can contribute to promoting sustainability by reducing the amount of energy consumed in the heating process.

4. EXPERIMENTAL SECTION

4.1. Materials. Cerium(III) nitrate hexahydrate (Aldrich), CDI (Aldrich), imidazole (Sigma-Aldrich), acetone (Sigma-Aldrich), hydrogen peroxide (Samchun), Amplex Red hydrogen peroxide/peroxidase assay kit (Invitrogen), and SOD assay kit (Dojindo Molecular Technologies, Inc.) were purchased and used without further purification.

4.2. Synthesis of CeCb Nanoplates and Nanosaucers. Synthetic conditions for each particle are summarized in Table 1. To synthesize CeCb nanoplates, a cerium nitrate hexahydrate precursor solution, prepared by dissolving 1 mmol cerium nitrate hexahydrate in 25 mL of acetone, and a CDI precursor solution, prepared by dissolving 4 mmol CDI in 25 mL of acetone, were mixed with vigorous stirring at room temperature. For the fabrication of CeCb nanosaucers, 2, 4, or 6 mmol imidazole were added into a reaction mixture containing 1 mmol cerium nitrate hexahydrate and 1 mmol CDI. Macaron-shaped CeCb microparticles were synthesized using the same as the abovementioned method for CeCb nanosaucers, except 1000 μL of deionized water was added. After mixing for 3 h at room temperature, the resulting precipitate was centrifuged, washed four times with deionized water, and dried at 60 °C for 12 h in air.

4.3. Conversion of CeCb Nanoparticles into CeONPs. To convert CeCb particles (nanoplates, nanosaucers, and macaron-shaped microparticles) into ceria particles, dried powdered CeCb particles were calcined in air for 2 h at 500 °C, as previously described.[23] The resulting ceria nanoparticles were designated as Cal-CeO nanoplates, Cal-CeO nanosaucers, or Cal-CeO micromacarons.

4.4. Direct Synthesis of CeONPs. Spherical CeONPs 130 nm in size were directly synthesized by reacting cerium nitrate hexahydrate, CDI, and imidazole in acetone. Typically, 1 mmol

https://doi.org/10.1021/acsomega.1c03700
ACS Omega 2021, 6, 26477−26488

cerium nitrate hexahydrate, 0.5 mmol CDI, and 4 mmol imidazole were dissolved in 25, 12.5, and 12.5 mL of acetone, respectively. The solutions of CDI and imidazole were sequentially added to a solution of cerium nitrate hexahydrate with vigorous stirring at room temperature. After mixing for 1 h, the precipitate was centrifuged, washed four times with deionized water, and dried at 60 °C in air for 12 h (designated as Ce-CDI-IM CeONPs). Spherical CeONPs 130 nm in size were also synthesized by mixing cerium nitrate hexahydrate and imidazole in acetone for 3 h without the addition of CDI in the aforementioned synthetic procedure. The resulting nanoparticles were designated as Ce-IM CeONPs.

4.5. Characterization. The morphology of the particles was evaluated using a JSM-6510 scanning electron microscope (SEM, JEOL) and a JEM-2100F transmission electron microscope (TEM) operating at 200 kV. The particle sizes were measured manually by ImageJ software (NIH) using 500 or more particles in SEM images. The hydrodynamic size and ζ-potential of the nanoparticles were analyzed using a Zetasizer Nano ZS90 (Malvern Panalytical). X-ray photoelectron spectroscopy (XPS) analysis was performed using an ESCALAB 250 (Thermo Scientific) and deconvolution of the XPS peaks was conducted using CasaXPS software (version 2.3.23PR1.0, Casa Software Ltd.) with a Shirley background and a Gaussian/Lorentzian (GL) line shape. X-ray powder diffraction (XRD) patterns of the samples were obtained using a diffractometer (D8 ADVANCE, Bruker Corporation). Fourier transform infrared (FTIR) spectra of the nanoparticles were obtained using an FTIR spectrometer (IFS-66/S, TENSOR27, Bruker). Thermogravimetric analysis (TGA) was conducted using a TG/DTA7300 (SEIKO Instruments) under a N_2 atmosphere at a heating rate of 10 °C/min.

4.6. Measurement of ROS-Scavenging Catalytic Properties. Catalase-mimicking activities of Ce-CDI-IM CeONPs, Ce-IM CeONPs, and Cal-CeONPs were measured using an Amplex Red hydrogen peroxide/peroxidase assay kit. Typically, various CeONPs were added in 1 mL of a 20 μM hydrogen peroxide solution using 24-well plates (final concentration: 100 μg/mL). The microplates were incubated for 1 h with gentle stirring and then 50 μL of samples from each well was transferred to 96-well plates. Then, 50 μL of a working solution containing the Amplex Red reagent (100 μM) and horseradish peroxidase (HRP, 0.2 U/mL) was added to each well. After incubation for another 30 min at room temperature to trigger the reaction between the Amplex Red reagent and hydrogen peroxide, the fluorescence of resorufin, the reaction product, was measured using wavelengths of 545 nm for excitation and 590 nm for emission by a Varioskan LUX multimode microplate reader (Thermo Fisher Scientific).

SOD-mimicking activity was determined by an SOD assay kit. Various CeONPs were added to 200 μL of the working solution for WST-1 (2-(4-iodophenyl)-3-(4-nitro-phenyl)-5-(2,4-disulfophenyl)-2*H*-tetrazolium, monosodium salt) in each well of the 96-well plates (final concentration: 100 μg/mL). Then, 20 μL of a xanthine oxidase (XO) solution was added to each well and microplates were incubated at 37 °C for 20 min. The absorbance of WST-1 formazan was measured using a microplate reader at 450 nm to determine the SOD activity as an inhibition activity.

■ ASSOCIATED CONTENT

Supporting Information

The Supporting Information is available free of charge at https://pubs.acs.org/doi/10.1021/acsomega.1c03700.

Additional data of SEM, XRD, particle sizes, and XPS about the reaction products (PDF)

Comparison of time points at which precipitation occurred during the reaction according to the amount of CDI (Video S1) (MP4)

Comparison of time points at which precipitation occurred during the reaction according to the amount of deionized water (Video S2) (MP4)

■ AUTHOR INFORMATION

Corresponding Author

Jaeyun Kim − *Department of Health Sciences and Technology, Samsung Advanced Institute for Health Sciences & Technology (SAIHST), Sungkyunkwan University (SKKU), Seoul 06355, Republic of Korea; School of Chemical Engineering, Biomedical Institute for Convergence at SKKU (BICS), and Institute of Quantum Biophysics (IQB), Sungkyunkwan University (SKKU), Suwon 16419, Republic of Korea;* orcid.org/0000-0002-4687-6732; Email: kimjaeyun@skku.edu

Author

Seung Woo Choi − *Department of Health Sciences and Technology, Samsung Advanced Institute for Health Sciences & Technology (SAIHST), Sungkyunkwan University (SKKU), Seoul 06355, Republic of Korea*

Complete contact information is available at: https://pubs.acs.org/10.1021/acsomega.1c03700

Notes

The authors declare no competing financial interest.

■ ACKNOWLEDGMENTS

This research was supported by the National Research Foundation (NRF) of Korea grants (Nos. 2019R1A2C2004765 and 2020M3A9D3039720) funded by the Korea government (MSIT) and the R&D Program for Forest Science Technology (No. 2020209B10-2122-BA01) provided by the Korea Forest Service (KFS) of the Korea Forestry Promotion Institute.

■ ABBREVIATIONS

ROS, reactive oxygen species; SOD, superoxide dismutase; CAT, catalase; CeONPs, cerium oxide nanoparticles; CeCbPs, cerium carbonate particles; CDI, 1,1′-carbonyldiimidazole; XPS, X-ray photoelectron spectroscopy; XRD, X-ray powder diffraction; SEM, scanning electron microscopy; TEM, transmission electron microscopy; FTIR, Fourier transform infrared; TGA, thermogravimetric analysis; DTG, derivative thermogravimetric

■ REFERENCES

(1) Trovarelli, A.; de Leitenburg, C.; Boaro, M.; Dolcetti, G. The utilization of ceria in industrial catalysis. *Catal. Today* **1999**, *50*, 353−367.

(2) Janoš, P.; Ederer, J.; Pilařová, V.; Henych, J.; Tolasz, J.; Milde, D.; Opletal, T. Chemical mechanical glass polishing with cerium

oxide: Effect of selected physico-chemical characteristics on polishing efficiency. *Wear* **2016**, *362*−*363*, 114−120.
(3) Ji, P.; Zhang, J.; Chen, F.; Anpo, M. Study of adsorption and degradation of acid orange 7 on the surface of CeO_2 under visible light irradiation. *Appl. Catal., B* **2009**, *85*, 148−154.
(4) Ishikawa, Y.; Takeda, M.; Tsukimoto, S.; Nakayama, K. S.; Asao, N. Cerium Oxide Nanorods with Unprecedented Low-Temperature Oxygen Storage Capacity. *Adv. Mater.* **2016**, *28*, 1467−1471.
(5) Bellon, O.; Sammes, N. M.; Staniforth, J. Mechanical properties and electrochemical characterisation of extruded doped cerium oxide for use as an electrolyte for solid oxide fuel cells. *J. Power Sources* **1998**, *75*, 116−121.
(6) Sun, C.; Li, H.; Chen, L. Nanostructured ceria-based materials: synthesis, properties, and applications. *Energy Environ. Sci.* **2012**, *5*, 8475−8505.
(7) Walkey, C.; Das, S.; Seal, S.; Erlichman, J.; Heckman, K.; Ghibelli, L.; Traversa, E.; McGinnis, J. F.; Self, W. T. Catalytic properties and biomedical applications of cerium oxide nanoparticles. *Environ. Sci.: Nano* **2015**, *2*, 33−53.
(8) Grulke, E.; Reed, K.; Beck, M.; Huang, X.; Cormack, A.; Seal, S. Nanoceria: factors affecting its pro- and anti-oxidant properties. *Environ. Sci.: Nano* **2014**, *1*, 429−444.
(9) Pirmohamed, T.; Dowding, J. M.; Singh, S.; Wasserman, B.; Heckert, E.; Karakoti, A. S.; King, J. E.; Seal, S.; Self, W. T. Nanoceria exhibit redox state-dependent catalase mimetic activity. *Chem. Commun.* **2010**, *46*, 2736−2738.
(10) Korsvik, C.; Patil, S.; Seal, S.; Self, W. T. Superoxide dismutase mimetic properties exhibited by vacancy engineered ceria nanoparticles. *Chem. Commun.* **2007**, *10*, 1056−1058.
(11) Jeong, H.-G.; Cha, B. G.; Kang, D.-W.; Kim, D. Y.; Yang, W.; Ki, S.-K.; Kim, S. I.; Han, J.; Kim, C. K.; Kim, J.; Lee, S.-H. Ceria Nanoparticles Fabricated with 6-Aminohexanoic Acid that Overcome Systemic Inflammatory Response Syndrome. *Adv. Healthcare Mater.* **2019**, *8*, No. 1801548.
(12) Kim, J.; Kim, H. Y.; Song, S. Y.; Go, S.-h.; Sohn, H. S.; Baik, S.; Soh, M.; Kim, K.; Kim, D.; Kim, H.-C.; Lee, N.; Kim, B.-S.; Hyeon, T. Synergistic Oxygen Generation and Reactive Oxygen Species Scavenging by Manganese Ferrite/Ceria Co-decorated Nanoparticles for Rheumatoid Arthritis Treatment. *ACS Nano* **2019**, *13*, 3206−3217.
(13) Naha, P. C.; Hsu, J. C.; Kim, J.; Shah, S.; Bouché, M.; Si-Mohamed, S.; Rosario-Berrios, D. N.; Douek, P.; Hajfathalian, M.; Yasini, P.; Singh, S.; Rosen, M. A.; Morgan, M. A.; Cormode, D. P. Dextran-Coated Cerium Oxide Nanoparticles: A Computed Tomography Contrast Agent for Imaging the Gastrointestinal Tract and Inflammatory Bowel Disease. *ACS Nano* **2020**, *14*, 10187−10197.
(14) Ni, D.; Wei, H.; Chen, W.; Bao, Q.; Rosenkrans, Z. T.; Barnhart, T. E.; Ferreira, C. A.; Wang, Y.; Yao, H.; Sun, T.; Jiang, D.; Li, S.; Cao, T.; Liu, Z.; Engle, J. W.; Hu, P.; Lan, X.; Cai, W. Ceria Nanoparticles Meet Hepatic Ischemia-Reperfusion Injury: The Perfect Imperfection. *Adv. Mater.* **2019**, *31*, No. 1902956.
(15) Oró, D.; Yudina, T.; Fernández-Varo, G.; Casals, E.; Reichenbach, V.; Casals, G.; González de la Presa, B.; Sandalinas, S.; Carvajal, S.; Puntes, V.; Jiménez, W. Cerium oxide nanoparticles reduce steatosis, portal hypertension and display anti-inflammatory properties in rats with liver fibrosis. *J. Hepatol.* **2016**, *64*, 691−698.
(16) Jeong, H.-G.; Cha, B. G.; Kang, D.-W.; Kim Do, Y.; Ki, S.-K.; Kim, S. I.; Han, J.; Yang, W.; Kim, C. K.; Kim, J.; Lee, S.-H. Ceria Nanoparticles Synthesized With Aminocaproic Acid for the Treatment of Subarachnoid Hemorrhage. *Stroke* **2018**, *49*, 3030−3038.
(17) Cha, B. G.; Jeong, H.-G.; Kang, D.-W.; Nam, M.-J.; Kim, C. K.; Kim, D. Y.; Choi, I.-Y.; Ki, S.-K.; Kim, S. I.; Han, Jh.; Kim, J.; Lee, S.-H. Customized lipid-coated magnetic mesoporous silica nanoparticle doped with ceria nanoparticles for theragnosis of intracerebral hemorrhage. *Nano Res.* **2018**, *11*, 3582−3592.
(18) Choi, S. W.; Kim, J. Recent Progress in Autocatalytic Ceria Nanoparticles-Based Translational Research on Brain Diseases. *ACS Appl. Nano Mater.* **2020**, *3*, 1043−1062.
(19) Choi, S. W.; Cha, B. G.; Kim, J. Therapeutic Contact Lens for Scavenging Excessive Reactive Oxygen Species on the Ocular Surface. *ACS Nano* **2020**, *14*, 2483−2496.
(20) Tisi, A.; Passacantando, M.; Lozzi, L.; Maccarone, R. Cerium oxide nanoparticles reduce the accumulation of autofluorescent deposits in light-induced retinal degeneration: Insights for age-related macular degeneration. *Exp. Eye Res.* **2020**, *199*, No. 108169.
(21) Kaczmarek, A. M.; Van Hecke, K.; Van Deun, R. Nano- and micro-sized rare-earth carbonates and their use as precursors and sacrificial templates for the synthesis of new innovative materials. *Chem. Soc. Rev.* **2015**, *44*, 2032−2059.
(22) Nakagawa, K.; Tezuka, Y.; Ohshima, T.; Katayama, M.; Ogata, T.; Sotowa, K.-I.; Katoh, M.; Sugiyama, S. Formation of cerium carbonate hydroxide and cerium oxide nanostructures by self-assembly of nanoparticles using surfactant template and their catalytic oxidation. *Adv. Powder Technol.* **2016**, *27*, 2128−2135.
(23) Janoš, P.; Henych, J.; Pfeifer, J.; Zemanová, N.; Pilařová, V.; Milde, D.; Opletal, T.; Tolasz, J.; Malý, M.; Štengl, V. Nanocrystalline cerium oxide prepared from a carbonate precursor and its ability to breakdown biologically relevant organophosphates. *Environ. Sci.: Nano* **2017**, *4*, 1283−1293.
(24) Sun, C.; Sun, J.; Xiao, G.; Zhang, H.; Qiu, X.; Li, H.; Chen, L. Mesoscale Organization of Nearly Monodisperse Flowerlike Ceria Microspheres. *J. Phys. Chem. B* **2006**, *110*, 13445−13452.
(25) He, Y.; Liang, X.; Chen, B. Globin-like mesoporous CeO_2: A CO-assisted synthesis based on carbonate hydroxide precursors and its applications in low temperature CO oxidation. *Nano Res.* **2015**, *8*, 1269−1278.
(26) Han, Z. H.; Guo, N.; Tang, K. B.; Yu, S. H.; Zhao, H. Q.; Qian, Y. T. Hydrothermal crystal growth and characterization of cerium hydroxycarbonates. *J. Cryst. Growth* **2000**, *219*, 315−318.
(27) Renuka, N. K.; Praveen, A. K.; Aniz, C. U. Ceria rhombic microplates: Synthesis, characterization and catalytic activity. *Microporous Mesoporous Mater.* **2013**, *169*, 35−41.
(28) Meher, S. K.; Ranga Rao, G. Tuning, via Counter Anions, the Morphology and Catalytic Activity of CeO_2 Prepared under Mild Conditions. *J. Colloid Interface Sci.* **2012**, *373*, 46−56.
(29) Li, Q.; Han, Z.; Shao, M.; Liu, X.; Qian, Y. Preparation of cerium hydroxycarbonate by a surfactant-assisted route. *J. Phys. Chem. Solids* **2003**, *64*, 295−297.
(30) Hirano, M.; Kato, E. Hydrothermal Synthesis of Two Types of Cerium Carbonate Particles. *J. Mater. Sci. Lett.* **1999**, *18*, 403−405.
(31) Qi, R.-J.; Zhu, Y.-J.; Cheng, G.-F.; Huang, Y.-H. Sonochemical synthesis of single-crystalline $CeOHCO_3$ rods and their thermal conversion to CeO_2 rods. *Nanotechnology* **2005**, *16*, 2502−2506.
(32) Riccardi, C. S.; Lima, R. C.; dos Santos, M. L.; Bueno, P. R.; Varela, J. A.; Longo, E. Preparation of CeO_2 by a simple microwave−hydrothermal method. *Solid State Ionics* **2009**, *180*, 288−291.
(33) Cui, M. Y.; He, J. X.; Lu, N. P.; Zheng, Y. Y.; Dong, W. J.; Tang, W. H.; Chen, B. Y.; Li, C. R. Morphology and size control of cerium carbonate hydroxide and ceria micro/nanostructures by hydrothermal technology. *Mater. Chem. Phys.* **2010**, *121*, 314−319.
(34) Tsai, M.-S. Powder synthesis of nano grade cerium oxide via homogenous precipitation and its polishing performance. *Mater. Sci. Eng., B* **2004**, *110*, 132−134.
(35) Tsai, M.-S. Formation of nanocrystalline cerium oxide and crystal growth. *J. Cryst. Growth* **2005**, *274*, 632−637.
(36) Sreekanth, T. V. M.; Nagajyothi, P. C.; Reddy, G. R.; Shim, J.; Yoo, K. Urea assisted ceria nanocubes for efficient removal of malachite green organic dye from aqueous system. *Sci. Rep.* **2019**, *9*, No. 14477.
(37) Chavhan, M. P.; Lu, C.-H.; Som, S. Urea and surfactant assisted hydrothermal growth of ceria nanoparticles. *Colloid Surf., A* **2020**, *601*, No. 124944.
(38) Tamizhdurai, P.; Sakthinathan, S.; Chen, S.-M.; Shanthi, K.; Sivasanker, S.; Sangeetha, P. Environmentally friendly synthesis of CeO_2 nanoparticles for the catalytic oxidation of benzyl alcohol to benzaldehyde and selective detection of nitrite. *Sci. Rep.* **2017**, *7*, No. 46372.

https://doi.org/10.1021/acsomega.1c03700
ACS Omega 2021, 6, 26477−26488

(39) Woodman, E. K.; Chaffey, J. G. K.; Hopes, P. A.; Hose, D. R. J.; Gilday, J. P. N,N′-Carbonyldiimidazole-Mediated Amide Coupling: Significant Rate Enhancement Achieved by Acid Catalysis with Imidazole·HCl. *Org. Process Res. Dev.* **2009**, *13*, 106−113.
(40) Lanzillotto, M.; Konnert, L.; Lamaty, F.; Martinez, J.; Colacino, E. Mechanochemical 1,1′-Carbonyldiimidazole-Mediated Synthesis of Carbamates. *ACS Sustainable Chem. Eng.* **2015**, *3*, 2882−2889.
(41) Montalbetti, C. A. G. N.; Falque, V. Amide bond formation and peptide coupling. *Tetrahedron* **2005**, *61*, 10827−10852.
(42) Staab, H. A. New Methods of Preparative Organic Chemistry IV. Syntheses Using Heterocyclic Amides (Azolides). *Angew. Chem., Int. Ed.* **1962**, *1*, 351−367.
(43) Rahaman, S. H.; Chowdhury, H.; Bose, D.; Mostafa, G.; Fun, H.-K.; Ghosh, B. K. 1D polymeric chain of copper(II) containing imidazolate and perchlorate bridging: Supramolecular synthon involving N−H···O hydrogen bonding. *Inorg. Chem. Commun.* **2005**, *8*, 1041−1044.
(44) Stamatatos, T. C.; Perlepes, S. P.; Raptopoulou, C. P.; Terzis, A.; Patrickios, C. S.; Tasiopoulos, A. J.; Boudalis, A. K. Alcoholysis/hydrolysis of 1,1′-carbonyldiimidazole as a means of preparing unprecedented, imidazole-containing one-dimensional coordination polymers of copper(II). *Dalton Trans.* **2009**, 3354−3362.
(45) Morsali, A.; Ranjbar, Z. R.; Amiri, M. G.; Askarinejad, A.; Xiao, H.-P. Synthesis, structural and spectroscopic characterization of a new cadmium(II) complex containing imidazole (Im) as ligand, $[Cd(Im)_6](ClO_4)_2$. *J. Coord. Chem.* **2006**, *59*, 961−967.
(46) Zhao, H.-Y.; Ma, J.-J.; Yang, X.-D.; Yang, M.-L. Synthesis, Crystal Structure, and Antibacterial Activity of a New Cobalt(II) Complex Containing Imidazole as Ligand. *Synth. React. Inorg., Met.-Org., Nano-Met. Chem.* **2016**, *46*, 45−50.
(47) Sadat, S. A.; Ghaedi, A. M.; Panahimehr, M.; Baneshi, M. M.; Vafaei, A.; Ansarizadeh, M. Rapid room-temperature synthesis of cadmium zeolitic imidazolate framework nanoparticles based on 1,1′-carbonyldiimidazole as ultra-high-efficiency adsorbent for ultrasound-assisted removal of malachite green dye. *Appl. Surf. Sci.* **2019**, *467−468*, 1204−1212.
(48) Park, K. S.; Ni, Z.; Côté, A. P.; Choi, J. Y.; Huang, R.; Uribe-Romo, F. J.; Chae, H. K.; O'Keeffe, M.; Yaghi, O. M. Exceptional chemical and thermal stability of zeolitic imidazolate frameworks. *Proc. Natl. Acad. Sci. U.S.A.* **2006**, *103*, No. 10186.
(49) Kida, K.; Okita, M.; Fujita, K.; Tanaka, S.; Miyake, Y. Formation of high crystalline ZIF-8 in an aqueous solution. *CrystEngComm* **2013**, *15*, 1794−1801.
(50) Motamedi, M.; Ramezanzadeh, M.; Ramezanzadeh, B.; Mahdavian, M. One-pot synthesis and construction of a high performance metal-organic structured nano pigment based on nanoceria decorated cerium(III)-imidazole network (NC/CIN) for effective epoxy composite coating anti-corrosion and thermo-mechanical properties improvement. *Chem. Eng. J.* **2020**, *382*, No. 122820.
(51) Carter, D. A.; Pemberton, J. E. Surface-enhanced Raman scattering of the acid-base forms of imidazole on silver. *Langmuir* **1992**, *8*, 1218−1225.
(52) Duboué-Dijon, E.; Mason, P. E.; Fischer, H. E.; Jungwirth, P. Changes in the hydration structure of imidazole upon protonation: Neutron scattering and molecular simulations. *J. Chem. Phys.* **2017**, *146*, No. 185102.
(53) Dai, Q.; Bai, S.; Li, H.; Liu, W.; Wang, X.; Lu, G. Template-free and non-hydrothermal synthesis of CeO_2 nanosheets via a facile aqueous-phase precipitation route with catalytic oxidation properties. *CrystEngComm* **2014**, *16*, 9817−9827.
(54) Oikawa, M.; Fujihara, S. Crystal growth of $Ce_2O(CO_3)_2·H_2O$ in aqueous solutions: Film formation and samarium doping. *J. Solid State Chem.* **2005**, *178*, 2036−2041.
(55) Ikuma, Y.; Oosawa, H.; Shimada, E.; Kamiya, M. Effect of microwave radiation on the formation of $Ce_2O(CO_3)_2·H_2O$ in aqueous solution. *Solid State Ionics* **2002**, *151*, 347−352.
(56) Park, I. Y.; Kim, D.; Lee, J.; Lee, S. H.; Kim, K.-J. Effects of urea concentration and reaction temperature on morphology of gadolinium compounds prepared by homogeneous precipitation. *Mater. Chem. Phys.* **2007**, *106*, 149−157.
(57) Kaczmarek, A. M.; Miermans, L.; Van Deun, R. Nano- and microsized Eu^{3+} and Tb^{3+}-doped lanthanide hydroxycarbonates and oxycarbonates. The influence of glucose and fructose as stabilizing ligands. *Dalton Trans.* **2013**, *42*, 4639−4649.
(58) Ward, M. R.; Jamieson, W. J.; Leckey, C. A.; Alexander, A. J. Laser-induced nucleation of carbon dioxide bubbles. *J. Chem. Phys.* **2015**, *142*, No. 144501.
(59) Crossno, S. K.; Kalbus, L. H.; Kalbus, G. E. Determinations of Carbon Dioxide by Titration: New Experiments for General, Physical, and Quantitative Analysis Courses. *J. Chem. Educ.* **1996**, *73*, No. 175.
(60) Minamidate, Y.; Yin, S.; Sato, T. Synthesis of Monodispersed rod-like and spherical CeO_2 particles by mild solution process. *IOP Conf. Ser.: Mater. Sci. Eng.* **2009**, *1*, No. 012003.
(61) Malek Khachatourian, A.; Golestani-Fard, F.; Sarpoolaky, H.; Vogt, C.; Toprak, M. S. Microwave assisted synthesis of monodispersed Y_2O_3 and Y_2O_3:Eu^{3+} particles. *Ceram. Int.* **2015**, *41*, 2006−2014.
(62) Sung, J. M.; Lin, S. E.; Wei, W. C. J. Synthesis and reaction kinetics for monodispersive Y_2O_3:Tb^{3+} spherical phosphor particles. *J. Eur. Ceram. Soc.* **2007**, *27*, 2605−2611.
(63) Zhang, T.; Wang, D.; Gao, Z.; Zhao, K.; Gu, Y.; Zhang, Y.; He, D. Performance optimization of a MnO_2/carbon nanotube substrate for efficient catalytic oxidation of low-concentration NO at room temperature. *RSC Adv.* **2016**, *6*, 70261−70270.
(64) Tang, Z.-X.; Yu, Z.; Zhang, Z.-L.; Zhang, X.-Y.; Pan, Q.-Q.; Shi, L.-E. Sonication-assisted preparation of CaO nanoparticles for antibacterial agents. *Quím. Nova* **2013**, *36*, 933−936.
(65) Yin, S.; Minamidate, Y.; Tonouchi, S.; Goto, T.; Dong, Q.; Yamane, H.; Sato, T. Solution synthesis of homogeneous plate-like multifunctional CeO_2 particles. *RSC Adv.* **2012**, *2*, 5976−5982.
(66) Blanco, E.; Shen, H.; Ferrari, M. Principles of nanoparticle design for overcoming biological barriers to drug delivery. *Nat. Biotechnol.* **2015**, *33*, 941−951.
(67) Holec, D.; Dumitraschkewitz, P.; Vollath, D.; Fischer, F. D. Surface Energy of Au Nanoparticles Depending on Their Size and Shape. *Nanomaterials* **2020**, *10*, No. 484.
(68) Shrestha, S.; Wang, B.; Dutta, P. Nanoparticle processing: Understanding and controlling aggregation. *Adv. Colloid Interface Sci.* **2020**, *279*, No. 102162.
(69) Pujar, M. S.; Hunagund, S. M.; Desai, V. R.; Patil, S.; Sidarai, A. H. One-step synthesis and characterizations of cerium oxide nanoparticles in an ambient temperature via Co-precipitation method. *AIP Conf. Proc.* **2018**, *1942*, No. 050026.
(70) Seo, J.; Lee, J. W.; Moon, J.; Sigmund, W.; Paik, U. Role of the Surface Chemistry of Ceria Surfaces on Silicate Adsorption. *ACS Appl. Mater. Interfaces* **2014**, *6*, 7388−7394.
(71) Ali, M. M.; Mahdi, H. S.; Parveen, A.; Azam, A. Optical properties of cerium oxide (CeO_2) nanoparticles synthesized by hydroxide mediated method. *AIP Conf. Proc.* **2018**, *1953*, No. 030044.
(72) Yan, B.; Zhu, H. Controlled synthesis of CeO_2 nanoparticles using novel amphiphilic cerium complex precursors. *J. Nanopart. Res.* **2008**, *10*, 1279−1285.
(73) Xia, X.; Lan, Y.; Li, J.; Chen, C.; Xu, B.; Luo, X.; Mao, X. Facile synthesis of nanoceria by a molten hydroxide method and its photocatalytic properties. *J. Rare Earths* **2020**, *38*, 951−960.
(74) Gulicovski, J. J.; Milonjić, S. K.; Szécsényi, K. M. Synthesis and Characterization of Stable Aqueous Ceria Sols. *Mater. Manuf. Processes* **2009**, *24*, 1080−1085.
(75) Raju, G. S. R.; Pavitra, E.; Yu, J. S. Facile template free synthesis of $Gd_2O(CO_3)_2·H_2O$ chrysanthemum-like nanoflowers and luminescence properties of corresponding Gd_2O_3:RE^{3+} spheres. *Dalton Trans.* **2013**, *42*, 11400−11410.
(76) Yin, J.; Li, C.; Chen, D.; Yang, J.; Liu, H.; Hu, W.; Shao, Y. Structure and dysprosium dopant engineering of gadolinium oxide nanoparticles for enhanced dual-modal magnetic resonance and fluorescence imaging. *Phys. Chem. Chem. Phys.* **2017**, *19*, 5366−5376.

https://doi.org/10.1021/acsomega.1c03700
ACS Omega 2021, 6, 26477−26488

(77) Janoš, P.; Kuráň, P.; Ederer, J.; Šťastný, M.; Vrtoch, L.; Pšenička, M.; Henych, J.; Mazanec, K.; Skoumal, M. Recovery of Cerium Dioxide from Spent Glass-Polishing Slurry and Its Utilization as a Reactive Sorbent for Fast Degradation of Toxic Organophosphates. *Adv. Mater. Sci. Eng.* **2015**, *2015*, No. 241421.
(78) Kar, S.; Patel, C.; Santra, S. Direct Room Temperature Synthesis of Valence State Engineered Ultra-Small Ceria Nanoparticles: Investigation on the Role of Ethylenediamine as a Capping Agent. *J. Phys. Chem. C* **2009**, *113*, 4862−4867.
(79) Zhang, F.; Wang, P.; Koberstein, J.; Khalid, S.; Chan, S.-W. Cerium oxidation state in ceria nanoparticles studied with X-ray photoelectron spectroscopy and absorption near edge spectroscopy. *Surf. Sci.* **2004**, *563*, 74−82.
(80) Zhou, Y.; Perket, J. M.; Zhou, J. Growth of Pt Nanoparticles on Reducible CeO_2 (111) Thin Films: Effect of Nanostructures and Redox Properties of Ceria. *J. Phys. Chem. C* **2010**, *114*, 11853−11860.
(81) Zhang, J.; Wong, H.; Yu, D.; Kakushima, K.; Iwai, H. X-ray photoelectron spectroscopy study of high-k CeO_2/La_2O_3 stacked dielectrics. *AIP Adv.* **2014**, *4*, No. 117117.
(82) Younis, A.; Chu, D.; Li, S. Oxygen level: the dominant of resistive switching characteristics in cerium oxide thin films. *J. Phys. D: Appl. Phys.* **2012**, *45*, No. 355101.
(83) Yang, C.; Yu, X.; Heißler, S.; Nefedov, A.; Colussi, S.; Llorca, J.; Trovarelli, A.; Wang, Y.; Wöll, C. Surface Faceting and Reconstruction of Ceria Nanoparticles. *Angew. Chem., Int. Ed.* **2017**, *56*, 375−379.
(84) Vinothkumar, G.; Arunkumar, P.; Mahesh, A.; Dhayalan, A.; Suresh Babu, K. Size- and defect-controlled anti-oxidant enzyme mimetic and radical scavenging properties of cerium oxide nanoparticles. *New J. Chem.* **2018**, *42*, 18810−18823.
(85) Barth, C.; Laffon, C.; Olbrich, R.; Ranguis, A.; Parent, P.; Reichling, M. A perfectly stoichiometric and flat CeO2(111) surface on a bulk-like ceria film. *Sci. Rep.* **2016**, *6*, No. 21165.
(86) Muñoz-Gil, D.; Figueiredo, F. M. L. High Surface Proton Conduction in Nanostructured ZIF-8. *Nanomaterials* **2019**, *9*, No. 1369.
(87) Zheng, W.; Tan, R.; Yin, S.; Zhang, Y.; Zhao, G.; Chen, Y.; Yin, D. Ionic liquid-functionalized graphene oxide as an efficient support for the chiral salen Mn (III) complex in asymmetric epoxidation of unfunctionalized olefins. *Catal. Sci. Technol.* **2015**, *5*, 2092−2102.
(88) Erdogan, N.; Bouziani, A.; Park, J.; Micusik, M.; Kim, S. Y.; Majkova, E.; Omastova, M.; Ozturk, A. Synthesis and enhanced photocatalytic activity of nitrogen-doped triphasic TiO_2 nanoparticles. *J. Photochem. Photobiol., A* **2019**, *377*, 92−100.
(89) Raza Naqvi, S. T.; Shirinfar, B.; Majeed, S.; Najam-ul-Haq, M.; Hussain, D.; Iqbal, T.; Ahmed, N. Synthesis, design and sensing applications of nanostructured ceria-based materials. *Analyst* **2018**, *143*, 5610−5628.
(90) Kockrick, E.; Schrage, C.; Grigas, A.; Geiger, D.; Kaskel, S. Synthesis and catalytic properties of microemulsion-derived cerium oxide nanoparticles. *J. Solid State Chem.* **2008**, *181*, 1614−1620.
(91) Amadine, O.; Essamlali, Y.; Fihri, A.; Larzek, M.; Zahouily, M. Effect of calcination temperature on the structure and catalytic performance of copper−ceria mixed oxide catalysts in phenol hydroxylation. *RSC Adv.* **2017**, *7*, 12586−12597.
(92) Kumar, S.; Srivastava, M.; Singh, J.; Layek, S.; Yashpal, M.; Materny, A.; Ojha, A. K. Controlled synthesis and magnetic properties of monodispersed ceria nanoparticles. *AIP Adv.* **2015**, *5*, No. 027109.
(93) Celardo, I.; De Nicola, M.; Mandoli, C.; Pedersen, J. Z.; Traversa, E.; Ghibelli, L. Ce^{3+} Ions Determine Redox-Dependent Anti-apoptotic Effect of Cerium Oxide Nanoparticles. *ACS Nano* **2011**, *5*, 4537−4549.
(94) Qin, H.; Tan, X.; Huang, W.; Jiang, J.; Jiang, H. Application of urea precipitation method in preparation of advanced ceramic powders. *Ceram. Int.* **2015**, *41*, 11598−11604.
(95) Thakur, N.; Manna, P.; Das, J. Synthesis and biomedical applications of nanoceria, a redox active nanoparticle. *J. Nanobiotechnol.* **2019**, *17*, No. 84.
(96) Bilecka, I.; Niederberger, M. New developments in the nonaqueous and/or non-hydrolytic sol−gel synthesis of inorganic nanoparticles. *Electrochim. Acta* **2010**, *55*, 7717−7725.
(97) Murphy, C. J. Sustainability as an emerging design criterion in nanoparticle synthesis and applications. *J. Mater. Chem.* **2008**, *18*, 2173−2176.
(98) Leng, W.; Pati, P.; Vikesland, P. J. Room temperature seed mediated growth of gold nanoparticles: mechanistic investigations and life cycle assesment. *Environ. Sci.: Nano* **2015**, *2*, 440−453.
(99) Długosz, O.; Banach, M. Inorganic nanoparticle synthesis in flow reactors − applications and future directions. *React. Chem. Eng.* **2020**, *5*, 1619−1641.
(100) Phillips, T. W.; Lignos, I. G.; Maceiczyk, R. M.; deMello, A. J.; deMello, J. C. Nanocrystal synthesis in microfluidic reactors: where next? *Lab Chip* **2014**, *14*, 3172−3180.
(101) Kumar, V.; Fustér, H. A.; Oh, N.; Zhai, Y.; Deshpande, K.; Shim, M.; Kenis, P. J. A. Continuous Flow Synthesis of Anisotropic Cadmium Selenide and Zinc Selenide Nanoparticles. *ChemNanoMat* **2017**, *3*, 204−211.

https://doi.org/10.1021/acsomega.1c03700
ACS Omega 2021, 6, 26477−26488